Power Electronics and Drives
Volume 8(43), 2023 DOI: 10.2478/pead-2023-0009

Power Electronics and Drives

State Estimation MRAS and Identification of Stator Winding Phase Fault Detection of the PMSG in Wind Energy Based on the Sliding Mode Control

Research paper

Samir Bouslimani[1], Samir Meradi[2,*], Said Drid[1], Larbi Chrifi-Alaoui[3], Ali Bezziane[1]

[1]*Higher National School of Renewable Energy, Environment and Sustainable Development, LSPIE Laboratory, Batna, Algeria*
[2]*Laboratory of Innovative Technologies, COSI Team, ENST, Algiers, Algeria*
[3]*Laboratory LTI, University of Picardie Jules Verne, Cuffies, Soissons, France*

Received: February 03, 2023; Accepted: March 18, 2023

Abstract: This paper proposes a method for the diagnosis of stator inter-turn short-circuit fault for permanent magnet synchronous generators (PMSG). Inter-turn short-circuit currents are among the most critical in PMSG. For safety considerations, a fast detection is required when a fault occurs. This approach uses the parameter estimation of the per-phase stator resistance in closed-loop control of variable speed of wind energy conversion system (WECS). In the presence of an incipient short-circuit fault, the estimation of the resistance of the stator in the d-q reference frame does not make it possible to give the exact information. To solve this problem, a novel fault diagnosis scheme is proposed using parameter estimation of the per-phase stator resistance. The per-phase stator resistance of PMSG is estimated using the MRAS algorithm technique in real time. Based on a faulty PMSG model expressed in Park's reference frame, the number of short-circuited turns is estimated using MRAS. Fault diagnosis is on line detected by analysing the estimated stator resistance of each phase according to the fault condition. The proposed fault diagnosis scheme is implemented without any extra devices. Moreover, the information on the estimated parameters can be used to improve the control performance. The simulation results demonstrate that the proposed method can estimate the faulty phase.

Keywords: *synchronous generators component • MRAS algorithm • stator inter-turn short-circuit fault • fault diagnosis*

1. Introduction

Nowadays, among the all renewable energy sources, wind systems are more economic in comparison with others. Variable wind speed systems deliver 20%–30% more energy in comparison with constant speed systems (Nguyen and Naidu, 2011). Many developed generation systems are used to extract maximum wind energy. To achieve the most efficient wind energy extraction system, it is recommended to run a wind turbine generator in a variable speed mode. This is because it allows for higher energy gain and reduced stresses on the system (Yin et al., 2007; Barut et al. 2018).

Permanent magnet synchronous machines (PMSM) are broadly used in different industrial fields as renewable energy (Costa et al., 2013; Weeber et al., 2010; Kallesoe et al. 2004). The development of rare-earth magnetic materials (such as neodymium magnets or samarium-cobalt magnets) for the manufacturing of permanent magnets makes PMSM highly competitive in terms of power density and efficiency (Wang and Deng, 2012; Yin et al., 2007), compared to other kind of machines; and due to the multitude of advantages they provide over other generator types, they have come to occupy a place of choice in the wind turbine market.

The presence of faults affects the efficiency of the motor drive, and thus early detection not only reduces repair costs but also energy losses. In electrical machines, one of the most critical faults is a break in the inter-turn insulation in the stator winding, generating an inter-turn short circuit (Beltran et al., 2009; Ekanayake et al., 2003).

* *Email: samir.meradi@enst.dz*

To avoid motor failure, it is important to have information on the state of health of the stator winding.

The majority of work carried out in the field of system monitoring and diagnostics, the tools used to detect and locate faults, are synthesised from an open-loop representation of the system. However, the reality of industrial applications means that systems are generally inserted in a regulation or control loop. Closed-loop diagnostics are particularly tricky for a number of reasons. On the one hand, the controller can mitigate the effect of faults, which makes their detection difficult. On the other hand, the system inputs being correlated with the outputs because of the looping creates a difficulty for localisation.

To detect inter-lap failures, there are two categories of detection: offline testing and online monitoring (Ameur et al., 2012; Brandao et al., 2008; Meradi et al. 2022). The first requires the engine to be taken out of service, while the second does not affect the continuation of the work (Amirat et al., 2009; Bonnett, 1978).

This paper presents robust control strategies of a permanent magnet synchronous generator (PMSG) wind energy conversion system (WECS) during inter-turn short-circuit fault and for maximum power extraction during wind speed variations.

With such technological improvements, classical controllers for WECSs can be updated by the development of more efficient strategies based on modern nonlinear control techniques such as Lyapunov control; such techniques have collectively emerged as a particularly suitable option to deal with electronically controlled variable-speed operating WECS.

2. System Description

The WECS consists of a wind turbine coupled to a PMSG to power a stand-alone system. A three-phase diode bridge rectifier is used for the AC/DC conversion. A boost converter (DC/DC) is used to vary the rotor speed (Meradi et al. 2013). The proposed control algorithm is independent on turbine characteristics, achieving the fast dynamic responses. A battery bank is also used to store surplus power and recompense when wind power is not enough for load demand (Figure 1).

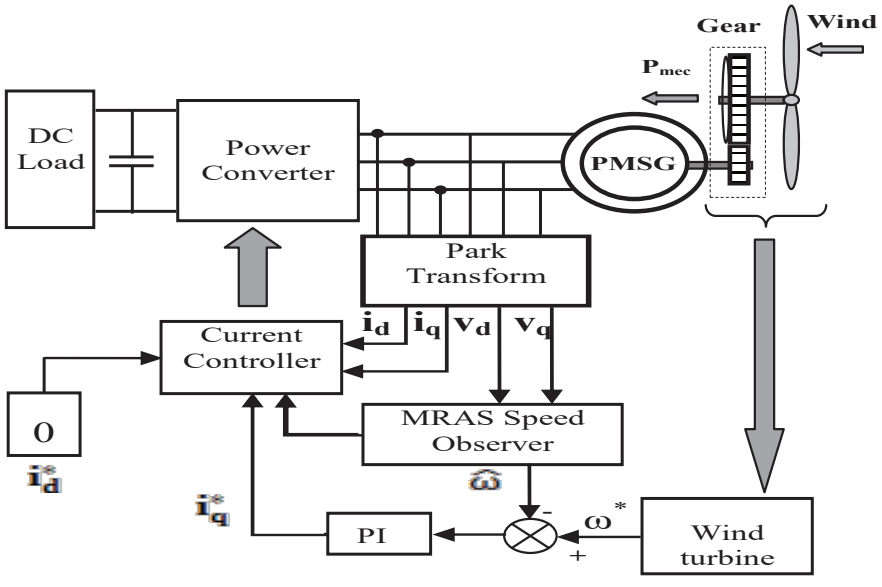

Fig. 1. Wind turbine control system. PMSG, permanent magnet synchronous generators; PI, proportional-integral control.

3. Wind Turbine Model

Several models for power production capability of wind turbines have been developed and can be found throughout the bibliography (see, in particular, Beltran et al. [2009] and Ekanayake et al. [2003]).

The mechanical power, captured by a wind turbine, depends on its power coefficient given for a wind velocity v and can be represented by:

$$P_{WT} = 0.5\pi\ \rho\, C_p(\lambda,\beta)\, R^2 V^3 \tag{1}$$

where ρ is the air density, R is the radius of wind turbine, V is the wind speed, and C_p is the power coefficient of wind turbine, which is a function of tip-speed ratio λ and pitch-angle β.

This C_p power coefficient is generally defined as a function of the tip-speed ratio λ, as can be inferred from Figure 2. In this research, a nonlinear empirical interpolation to represent the C_p is employed as follows (Ekanayake et al., 2003):

$$\begin{cases} C_p = 7.9563\times10^{-5}\lambda^5 - 17.375\times10^{-4}\lambda^4 + 9.86\times10^{-3}\lambda^3 \\ \qquad -9.4\times10^{-3}\lambda^2 + 6.38\times10^{-2}\lambda + 0.001 \\ \lambda = \dfrac{\omega_{WT} R}{v} \end{cases} \tag{2}$$

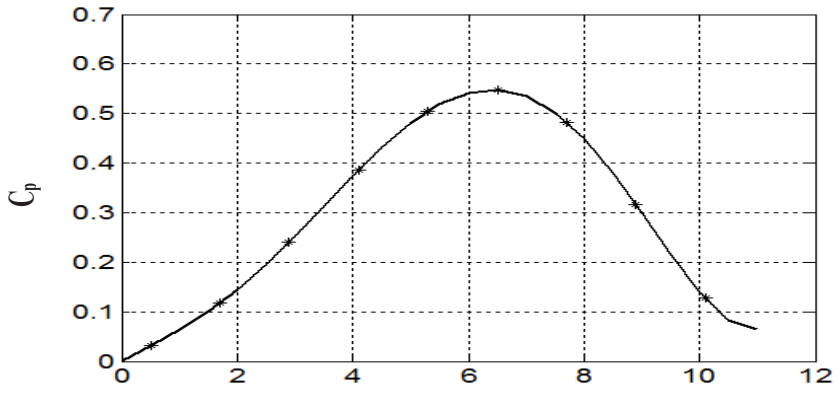

Fig. 2. Turbine power coefficient various tip-speed-ratio characteristic.

4. PMSG Modelling

The control objective of the generator-side converter is to extract the maximum power for the PMSG system (Fetene and Shibeshi 2020). The nonlinear control based on Lyapunov theory for the Generator magnet synchronous machines (GMSM) algorithm is applied to control the speed of the PMSG according to its reference speed, which is calculated by the maximum power point tracking (MPPT) control.

The electrical model in the d-q frame of PMSG can be expressed as:

$$\begin{cases} \dfrac{dI_d}{dt} = -\dfrac{R_s}{L_d} I_d + \dfrac{L_q}{L_d} I_q\, \omega - \dfrac{v_d}{L_d} \\ \dfrac{dI_q}{dt} = -\dfrac{R_s}{L_q} I_q - \dfrac{L_d}{L_q}\omega\, I_d + \dfrac{\Phi_f}{L_q}\omega - \dfrac{v_q}{L_q} \end{cases} \tag{3}$$

where I_d and I_q are stator currents in a rotating reference frame (the d-q reference frame), R_d and R_q are stator resistances, L_d and L_q are d-q reference frame stator inductances, ω is the electrical rotor speed, v_d and v_q are stator voltages in the d-q reference frame, and ϕ_f is a permanent magnet flux of rotor.

The expression for the electromagnetic torque can be described as:

$$T_e = \frac{3}{2} p\left[\varphi_f I_q - (L_d - L_q) I_d I_q\right] \tag{4}$$

The dynamic equation of the wind turbine is described by:

$$J\frac{d\Omega_g}{dt} = T_e - T_m - F.\Omega_g \tag{5}$$

where J is the moment of inertia, F is the viscous friction coefficient, and T_m is the mechanical torque developed by the turbine.

The produced electrical power and reactive powers are given, respectively, by:

$$\begin{aligned} P &= \frac{3}{2}\left(V_d I_d + V_q I_q\right) \\ Q &= \frac{3}{2}\left(V_q I_d + V_d I_q\right) \end{aligned} \tag{6}$$

Therefore, the active and reactive power can be controlled by controlling the direct and quadrature currents, respectively. However, in the presence of large inductive, or capacitive, loads, an additional source of reactive power is required to avoid generation–demand mismatch of reactive power to maintain the system voltage within acceptable limits.

5. A Nonlinear Control Strategy

The suggested PMSG control scheme is shown in Figure 1. We can also note the placement of the estimator block, which evaluates the feedback function in terms of f_d and f_q given by:

$$\begin{aligned} f_d &= -\frac{R_s}{L_d} I_d + \frac{L_q}{L_d} I_q\, \omega \\ f_q &= -\frac{R_s}{L_q} I_q - \frac{L_d}{L_q}\omega\, I_q + \frac{\varphi_f}{L_q}\omega \end{aligned} \tag{7}$$

To determine the control feedback, we rewrite Eq. (3) as the following:

$$\begin{cases} \dfrac{dI_d}{dt} = \lambda_d v_d + f_d \\ \dfrac{dI_q}{dt} = \lambda_q v_q + f_q \end{cases} \tag{8}$$

with $\lambda_d = -1/L_d$ and $\lambda_q = -1/L_q$

The nonlinear functions f_d and f_q involved in the state-space model (8) are strongly affected by the conventional effects of PMSG.

$$\begin{cases} \dfrac{dI_d}{dt} = \lambda_d v_d + \hat{f}_d + \Delta f_d \\ \dfrac{dI_q}{dt} = \lambda_q v_q + \hat{f}_q + \Delta f_q \end{cases} \tag{9}$$

Let the candidate Lyapunov function related to the currents dynamics be defined by:

$$V = \frac{1}{2} e_d^2 + \frac{1}{2} e_q^2 > 0 \tag{10}$$

with: $e_d = I_d - I_{d\_\mathrm{ref}}$ and $e_q = I_q - I_{q\_\mathrm{ref}}$

This function is globally positive defined over the whole state space. Its derivative is given by:

$$\dot{V} = e_d\, \dot{e}_d + e_q\, \dot{e}_q \tag{11}$$

Inserting Eq. (9) in Eq. (11) we obtain:

$$\begin{aligned}\dot{V} &= \left(\lambda_d v_d + f_d + \Delta f_d - \dot{I}_{d\_\mathrm{ref}}\right) e_d \\ &\quad + \left(\lambda_q v_q - f_q + \Delta f_q - \dot{I}_{q\_\mathrm{ref}}\right) e_q\end{aligned} \tag{12}$$

selecting the control law as:

$$\begin{cases} v_d = \dfrac{1}{\lambda_d}(-\hat{f}_d + \dot{I}_{d\_ref} - K_1\, e_d - K_{11}\,\mathrm{sgn}\,(e_d)) \\ v_q = \dfrac{1}{\lambda_q}(-\hat{f}_q + \dot{I}_{q\_ref} - K_2\, e_q - K_{22}\,\mathrm{sgn}\,(e_q)) \end{cases} \tag{13}$$

where K_{11} and $K_{22} > \beta_i$

New entries must be designed to ensure that:

$$\begin{cases} \lim\limits_{t\to+\infty}(I_d - I_{d\_ref}) = 0 \\ \lim\limits_{t\to+\infty}(\Omega - \Omega_{ref}) = 0 \end{cases}$$

Inserting the control law (13) in (12), we obtain:

$$\begin{aligned}\dot{V}_1 &= e_d\,\left(\Delta f_d - K_{11}\mathrm{sign}\,(e_d)\right) \\ &\quad + e_q\,\left(\Delta f_q - K_{22}\mathrm{sign}\,(e_q)\right) + \dot{V} < 0\end{aligned} \tag{14}$$

where $\dot{V}$ is given by:

$$\dot{V} = -K_1 e_d^2 - K_2 e_q^2 < 0 \tag{15}$$

Therefore, the Δf_d and Δf_q variations can be absorbed if we take:

$$K_{11} > |\Delta f_d|$$
$$K_{22} > |\Delta f_q|$$

These inequalities are satisfied if $K_{1,2} > 0$ and

$$|\Delta f| < \beta < K_{11,22}\,.$$

Finally, we can write: $\dot{V}_1 < \dot{V} < 0$ and

$$\begin{cases} lim\limits_{t\to+\infty}(I_d - I_{d\_\mathrm{ref}}) = 0 \\ lim\limits_{t\to+\infty}(I_q - I_{q\_\mathrm{ref}}) = 0 \end{cases}$$

5.1. Robust control in state space

The problem of robust scaling of the state setting is to resort to the principle of imposing a pole domain. In this case one does not impose poles well distinct, but a certain admissible domain in the plane S. Therefore, one also obtains a certain corresponding domain for the closed-loop coefficients in the space P as well as a domain for the coefficients of the state feedback in the space R (Figure 3). In this domain, which depends on the variable parameters K of the system, one can then choose the fixed coefficients of the state feedback. Since it is necessary to determine the domain of the coefficients for several parameters, one speaks of a problem involving multi-models, where it is necessary to treat several models for the system to be regulated having different parameters (Ackermann, 1980, 1985).

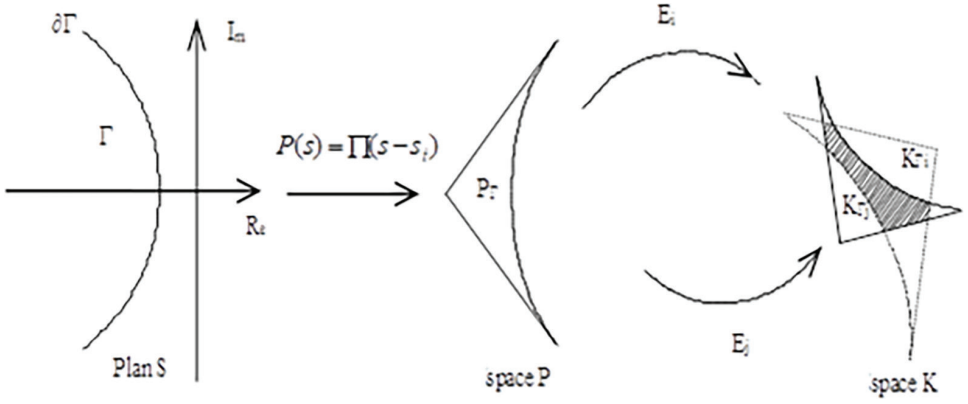

Fig. 3. The transition between stability regions (Γ ® PΓ ® KΓ).

The objective is to determine the coefficients of the state regulator in such a way that the roots of the closed-loop characteristic equation lie in the left half-plane of the complex plane, regardless of the values of the physical parameters. To achieve this goal, we need to examine the stability images and regions associated with the K and R regions (in the S plane) in the spaces corresponding to the Kinter section of the stability regions. This analysis provides a solution to the problem of robustness with respect to the physical parameter in question. The state regulator computed using this approach must exhibit satisfactory performance for all possible values of the robust coefficients within the domain of validity (as defined by Ackermann, 1985; Ghosh, 1986).

5.2. Region of stability in space

The characteristic closed-loop equation is:

$$P(s) = \sum_{i=0}^{n} \alpha_i s^i = \prod_{i=1}^{n} (s - s_i) = \begin{pmatrix} \alpha^t & 1 \end{pmatrix} s_n \tag{16}$$

with:

$$\alpha^t = \begin{pmatrix} \alpha_0 & . & . & . & \alpha_{n-1} \end{pmatrix}$$

$$\text{and} \quad s_n = \begin{pmatrix} 1 & s & . & . & . & s^n \end{pmatrix}^t$$

The α_i are the coordinates of the vector α^t, which represents a point in space P of dimension n.

It follows that [21]:

$$\alpha \in \mathrm{P}_\Gamma \Leftrightarrow z_i \in \Gamma \quad \forall i = \overline{1,n} \tag{17}$$

as P_r is the region of stability in space P. P_r is limited by a real surface and a complex surface.

The limit of the real pole, defined by the contour intersection $\partial\Gamma$ with the axis of the reals, is given by the equation of the following hyperplane (Ackermann, 1980):

$$\begin{aligned} &P(-\rho) = \sum (-1)^i \alpha_i \rho_0^i = \begin{pmatrix} \alpha^t & 1 \end{pmatrix} a_0 \\ &\text{with}: \quad a_0 = \begin{pmatrix} 1 & -\rho & . & . & . & -(1)^n \rho^n \end{pmatrix}^t \end{aligned} \tag{18}$$

On the other hand, the complex limit describes all the polynomials that have at least one pair of complex poles conjugated in the outline $\partial\Gamma$. For a pair of complex conjugate poles: $s_{1,2} = -\rho \pm j\omega$, the corresponding characteristic polynomial is:

$$Q(s) = (s - s_1)(s - s_2) = s^2 + 2\rho s + \rho^2 + \omega^2 = s^2 + \beta_1 s + \beta_0 \tag{19}$$

with:

$$\beta_1 = 2\rho \quad \text{and} \quad \beta_0 = \rho^2 + \omega^2$$

and thus P (s) is written as:

$$P(s) = \left(\beta_0 + \beta_1 s + s^2\right)\left(\sum_{i=0}^{n-3} \delta_i s^i + s^{n-2}\right) \tag{20}$$

In a matrix form:

$$\begin{aligned} &\left(\alpha^t \quad 1\right) s_n = \left(\beta_0 \quad \beta_1 \quad 1\right) s_2 \left(\delta^t \quad 1\right) s_{n-2} \\ &\text{or } \delta = \left(\delta_0 \quad . \quad . \quad . \quad \delta_{n-3}\right)^t \end{aligned} \tag{21}$$

By eliminating the vector S_n of the two members, we will have:

$$\left(\alpha^t \quad 1\right) = \left(\delta^t \quad 1\right) \begin{pmatrix} \beta_0 & \beta_1 & 1 & 0 & 0 & . & . & . & 0 \\ 0 & \beta_0 & \beta_1 & 1 & 0 & . & . & . & 0 \\ . & . & . & . & . & . & . & . & . \\ . & . & . & . & . & . & . & . & . \\ . & . & . & . & . & . & . & . & . \\ 0 & 0 & 0 & . & . & . & \beta_1 & 1 & 0 \\ 0 & 0 & 0 & . & . & . & \beta_0 & \beta_1 & 1 \end{pmatrix} \tag{22}$$

In order to eliminate the unknown δ, Eq. (23) can be put in the following form:

$$\left(\alpha^t \quad 1\right) = \left(0 \quad 0 \quad \delta^t \quad 1\right) \begin{pmatrix} 1 & 0 & 0 & . & . & . & 0 & 0 \\ \beta_1 & 1 & 0 & . & . & . & 0 & 0 \\ \beta_0 & \beta_1 & 1 & . & . & . & . & . \\ . & . & . & . & . & . & . & . \\ . & . & . & . & . & . & . & . \\ . & . & . & . & . & . & . & . \\ 0 & 0 & . & . & . & \beta_1 & 1 & 0 \\ 0 & 0 & . & . & . & \beta_0 & \beta_1 & 1 \end{pmatrix} \tag{23}$$

therefore:

$$\left(0 \quad 0 \quad \delta^t \quad 1\right) = \left(\alpha^t \quad 1\right) \beta^{-1} \tag{24}$$

with:

$$\beta = \begin{pmatrix} 1 & 0 & . & . & . & . & 0 & 0 \\ \beta_1 & 1 & . & . & . & . & 0 & 0 \\ \beta_0 & \beta_1 & . & . & . & . & . & . \\ . & . & . & . & . & . & . & . \\ . & . & . & . & . & . & . & . \\ . & . & . & . & . & . & . & . \\ 0 & 0 & . & . & . & \beta_1 & 1 & 0 \\ 0 & 0 & . & . & . & \beta_0 & \beta_1 & 1 \end{pmatrix}$$

Any calculation done gives:

$$\beta^{-1} = \begin{pmatrix} 1 & 0 & . & . & . & . & 0 & 0 \\ d_1 & 1 & . & . & . & . & 0 & 0 \\ d_2 & d_1 & . & . & . & . & . & . \\ . & . & . & . & . & . & . & . \\ . & . & . & . & . & . & . & . \\ . & . & . & . & . & . & . & . \\ . & . & . & . & . & d_1 & 1 & 0 \\ d_n & . & . & . & . & d_2 & d_1 & 1 \end{pmatrix} \tag{25}$$

The d_i are given by the following recursive form:

$$\begin{cases} d_0 = 1 \\ d_1 = -\beta_1 \\ d_{i+1} = -\beta_1 d_i - \beta_0 d_{i-1}, \quad i = \overline{1, n-1} \end{cases} \tag{26}$$

From Eq. (24), we can write:

$$\begin{pmatrix} \alpha^t & 1 \end{pmatrix} \begin{pmatrix} 1 & 0 \\ d_1 & 1 \\ d_2 & d_1 \\ . & . \\ . & . \\ . & . \\ d_n & d_{n-1} \end{pmatrix} = \begin{pmatrix} 0 & 0 \end{pmatrix} \tag{27}$$

with:

$$c_1 = \begin{pmatrix} d_0 & . & . & . & d_n \end{pmatrix}^t \quad \text{et} \quad c_2 = \begin{pmatrix} 0 & d_0 & . & . & . & d_n \end{pmatrix}^t$$

The complex limit will therefore be: the intersection of two hyperplanes of dimensions (n–1). It is given by:

$$\begin{pmatrix} \alpha^t & 1 \end{pmatrix} \begin{pmatrix} c_1 & c_2 \end{pmatrix} = \begin{pmatrix} 0 & 0 \end{pmatrix} \tag{28}$$

5.3. Region of stability in space K

If certain conditions or values in space P are necessary for stability, then it is important to determine which coefficients in space K will lead to those conditions or values.

From Eq. (28), the vector α^t is calculated by the following expression:

$$\alpha^t = k^t W + a^t \tag{29}$$

By injecting this equation into Eqs (19) and (29), it follows that [21]:

$$\begin{aligned} &\begin{pmatrix} a^t + k^t W & 1 \end{pmatrix} a_0 = 0 \\ &\begin{pmatrix} a^t + k^t W & 1 \end{pmatrix} \begin{pmatrix} c_1 & c_2 \end{pmatrix} = \begin{pmatrix} 0 & 0 \end{pmatrix} \end{aligned} \tag{30}$$

This equation allows us to graphically present the region of stability in space K.

6. Application on the Permanent Magnet Synchronous Machine

Figure 4 presents a block diagram of the speed control, by a robust pole-positioning state regulator, of a PMSM supplied by a voltage inverter controlled by the pulse width modulation (PWM) technique (the triangulo strategy – sinusoidal).The regulator must be associated with an anti-windup system in order to avoid an overshoot because the integrator would continue to sum an error that no longer corresponds to the control voltage. The correction of the integral component gives:

$$x_r[k+1] = x_r[k] + \frac{v_{qs}^{\lim}[k] - v_{qs}[k]}{k_w} \tag{31}$$

The augmented system with an integrating regulator is given by Eq. (31).

By applying the Leverrier algorithm, the vector coefficients of the closed-loop characteristic equation are given by:

$$\frac{d}{dt}\begin{pmatrix} i_{qs} \\ \omega_r \\ x_r \end{pmatrix} = \begin{pmatrix} -\frac{R}{L_q} - \frac{K_1}{L_q} & -\frac{\varphi_f^*}{L_q} - \frac{K_2}{L_q} & \frac{K_r}{L_q} \\ \frac{\varphi_f^* p^2}{J} & -\frac{f}{J} & 0 \\ 0 & -\frac{1}{T_i} & 0 \end{pmatrix} \begin{pmatrix} i_{qs} \\ \omega_r \\ x_r \end{pmatrix} + \begin{pmatrix} \frac{K_w}{L_q} \\ 0 \\ \frac{1}{T_i} \end{pmatrix} \omega_m^* + \begin{pmatrix} -\frac{K_v}{L_q} \\ -\frac{p}{J} \\ 0 \end{pmatrix} C_r \tag{32}$$

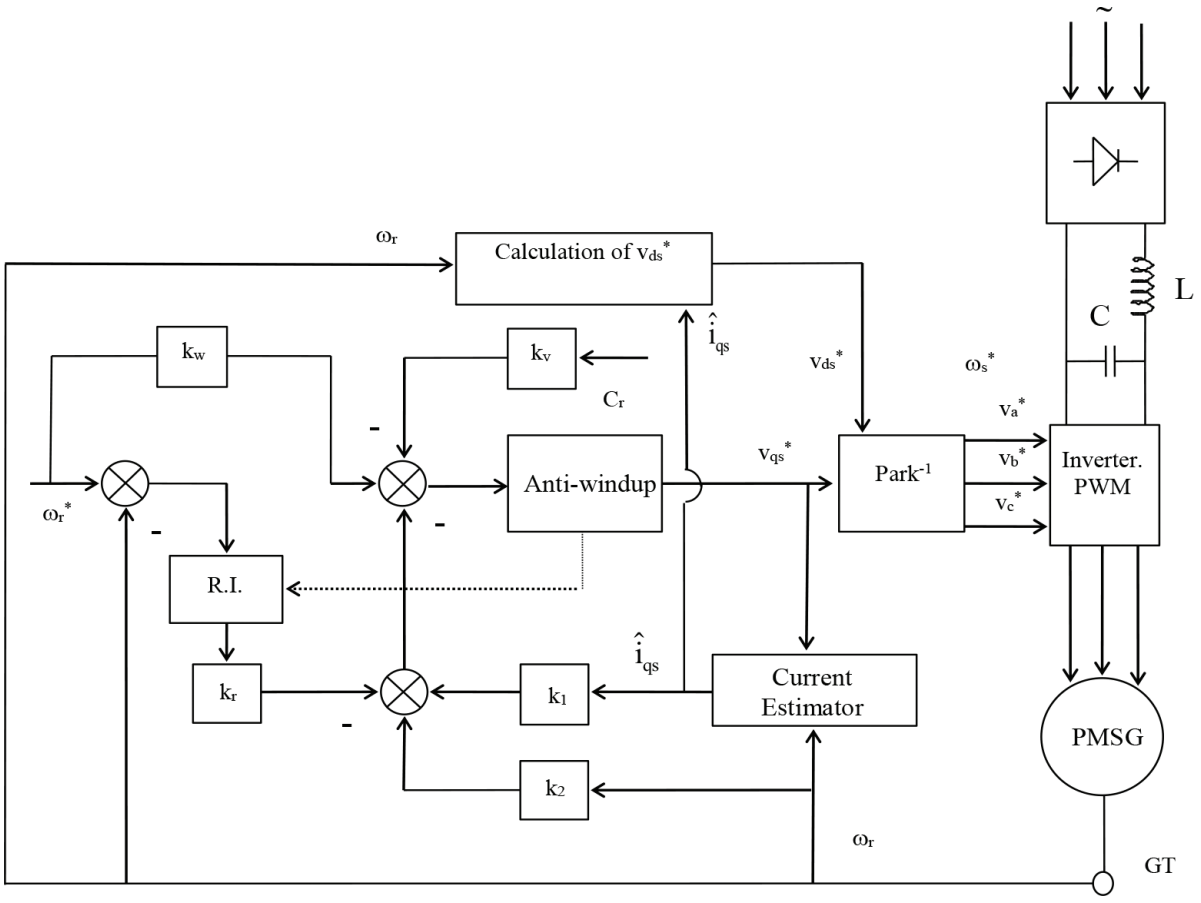

Fig. 4. Block diagram of the speed control by state feedback of a PMSG. PMSG, permanent magnet synchronous generators.

The region of stability in the plane S retained is represented by Figure 5:

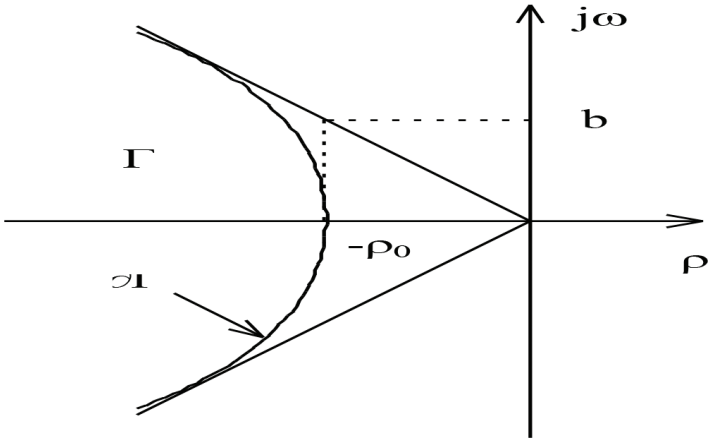

Fig. 5. Region of stability in the S plane.

This region of stability is described by the following hyperbola equation:

$$\partial\Gamma: \quad \left(\frac{\rho}{a}\right)^2 - \left(\frac{\omega}{b}\right)^2 = 1 \quad ; \quad \rho \le -a$$
$$\text{With}: \quad a = \rho_0 \quad et \quad b^2 = \rho_0^2 \frac{1-\xi^2}{\xi^2} \tag{33}$$

where ξ represents the relative damping coefficient.

In order to have the image of this region in the space K, it is necessary to calculate, on the one hand, the complex limit traced by the movement of a pair of complex conjugate poles along the contour, and on the other hand, the real limit that presents the image of a fixed pole at -ρ0 in the space K.

The coefficients β_i are given by:

$$\beta_1 = 2\rho \quad \text{et} \quad \beta_0 = \rho^2 + \omega^2 = \left(\left(\frac{b}{a}\right)^2 + 1\right)\rho^2 - b^2 \tag{34}$$

The complex limit is defined, in the space P, by:

$$\begin{pmatrix} \alpha^t & 1 \end{pmatrix} \begin{pmatrix} 1 & 0 \\ 0 & 1 \\ -\beta_0 & -\beta_1 \\ \beta_0\beta_1 & \beta_1^2 - \beta_0 \end{pmatrix} = \begin{pmatrix} 0 & 0 \end{pmatrix} \tag{35}$$

In order to have a two-dimensional representation in the space K, we will eliminate the contribution of the current iqs in the control law (K_1 = 0). The expansion of Eq. (35) gives:

$$K_r = -\frac{T_i \sigma L_s L_r J}{L_m j^*_r p^2} \beta_0 \left(\beta_1 - \left(\frac{R_{eq}}{\sigma L_s} + \frac{f}{J}\right)\right)$$
$$K_2 = \frac{\sigma L_s L_r J}{L_m \varphi^*_r p^2} \left(-\beta_1 \left(\beta_1 - \left(\frac{R_{eq}}{\sigma L_s} + \frac{f}{J}\right)\right) + \beta_0 - \frac{(\varphi^*_r p)^2}{\sigma L_r J} - \frac{f R_{eq}}{\sigma L_s J}\right) \tag{36}$$

As for the actual limit, this limit is defined in the space R by the following equation:

$$\begin{pmatrix} \alpha^t & 1 \end{pmatrix} \begin{pmatrix} 1 \\ -\rho_0 \\ \rho_0^2 \\ -\rho_0^3 \end{pmatrix} = 0 \tag{37}$$

If we consider that $K_1 = 0$, it happens that:

$$K_2 = \frac{K_r}{T_i \rho_0} - \frac{L_q J}{\varphi_f^* p^2} \left(\frac{fR}{L_q J} + \frac{(\varphi_f^* p)^2}{L_q J} + \rho_0^2 - \left(\frac{R}{L_q} + \frac{f}{J} \right) \rho_0 \right) \tag{38}$$

6.1. Robust sizing against *j*

The calculation methodology is identical to that presented above. Assuming that the variation of the moment of inertia can be modelled by the following discrete values (100%, 125%, 150%, 175%, 200%)Jn., the corresponding regions of stability would then be bounded by:

– The complex limit:

$$K_2 = \frac{L_q J^i}{\varphi_f^* p^2} \left(-\beta_1 \left(\beta_1 - \left(\frac{R}{L_q} + \frac{f}{J^i} \right) + \beta_0 - \frac{(\varphi_f^* p)^2}{L_q J^i} - \frac{fR}{L_q J^i} \right) \right) \tag{39}$$

– The actual limit:

$$K_2 = \frac{K_r}{T_i \rho_0} - \left(\frac{fR}{L_q J^i} + \frac{(\varphi_f^* p)^2}{L_q J^i} - \rho_0 \left(\frac{R}{L_q} + \frac{f}{J^i} \right) + \rho_0^2 \right) \frac{J^i L_q}{\varphi_f^* p^2} \tag{40}$$

$$\text{With: } \begin{cases} J^1 = J^n \\ J^{i+1} = J^i + 0.25 J^n \quad i = \overline{1,4} \end{cases} \tag{41}$$

The intersection of the different regions in the plane K is given by the domain as it is represented in Figure 6.

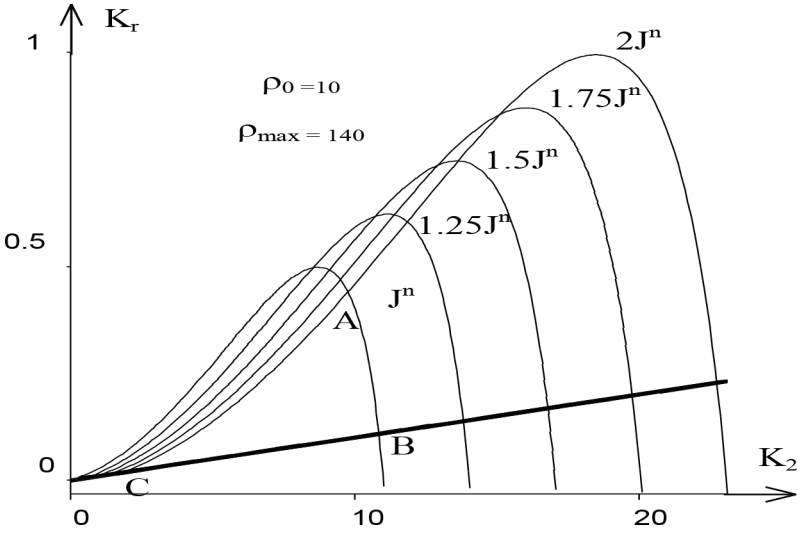

Fig. 6. Domain of the coefficients of the state adjustment in the plane (K_r, K_2).

6.1.1. Calculation of K_w

The pole to be compensated is given by:

$$S_{cg} = -\frac{1}{3(J^{\max} - J^{\min})} \int_{J^{\min}}^{J^{\max}} \left(\frac{R}{L_q} + \frac{f}{J} \right) dJ \tag{42}$$

With $J\max = 2Jn$ and $J\min = Jn$, we have:

$$K_w = \frac{3K_r}{T_i \left(\frac{R}{L_q} + \frac{f \ln(2)}{J^n} \right)} \tag{43}$$

6.1.2. Calculation of K_v

For the calculation of the coefficient of the direct intervention of the disturbance quantity based on the cancellation of the state of the integrating regulator in steady state, we adopt its nominal value calculated by the equation:

$$K_v = -\frac{R_{eq} L_r}{L_m \varphi_r^* p} \tag{44}$$

To obtain the gains of the digital regulator, the following correction must be made to the coefficients of the continuous regulator (Robyns, 1992):

$$\begin{aligned} &k_2 = K_2 + \frac{K_r}{2} \quad ; \quad k_r = K_r \\ &k_w = K_w + \frac{K_r}{2} \quad ; \quad k_v = K_v \\ &T_i = T_e (\text{sample period e} = 1 \text{ ms}) \end{aligned} \tag{45}$$

7. Estimation of R_s by Classical MRAS Technique

The system (3) is considered as the model reference and the observer is used as the adjustable one (Hajji et al. 2020). The stator resistance is included in Eq. (14), which represents a current model relevant to stator resistance. So, the stator current model is chosen as the state variable:

$$\begin{aligned} \frac{d\hat{I}_d}{dt} &= -\frac{\hat{R}_s}{L_d} \hat{I}_d + \frac{L_q}{L_d} \hat{I}_q \, \omega - \frac{v_d}{L_d} \\ \frac{d\hat{I}_q}{dt} &= -\frac{\hat{R}_s}{L_q} \hat{I}_q - \frac{L_d}{L_q} \omega \, \hat{I}_d + \frac{\Phi_f}{L_q} \omega - \frac{v_q}{L_q} \end{aligned} \tag{46}$$

The stator resistance is built around the following adaptive mechanism as (Utkin et al., 2009):

$$\hat{R}_s = -\frac{1}{L_d} \int \left(e_d \, \hat{i}_{ds} + e_q \, \hat{i}_{qs} \right) dt \tag{47}$$

with:

$$e_d = (I_d - \hat{I}_d); e_q = (I_q - \hat{I}_q)$$

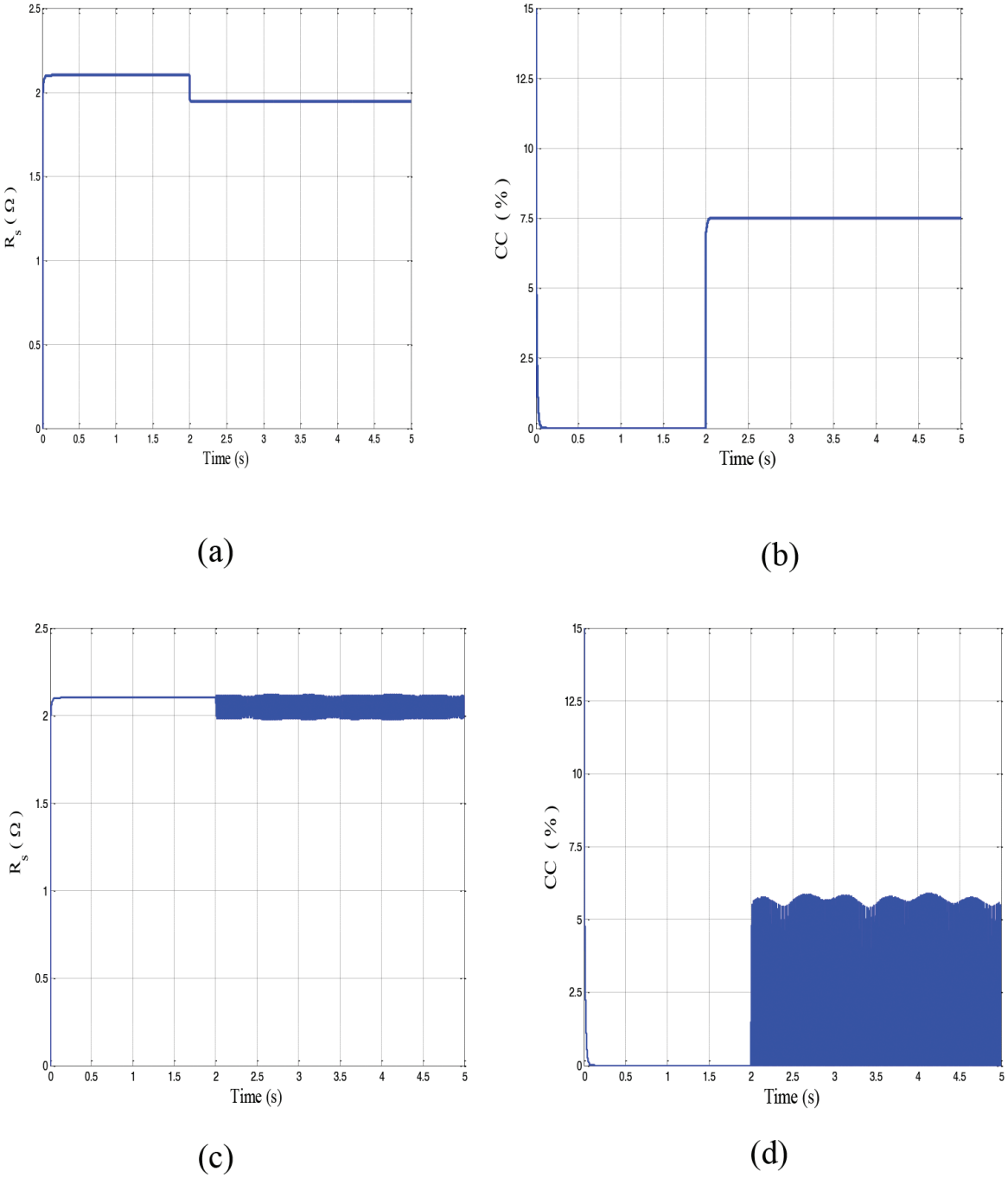

Fig. 7. (a) Stator resistance estimation under inter-turn short-circuit fault, (b) inter turn short circuit indicator, (c) stator resistance estimation under inter-turn short-circuit fault, and (d) inter turn short circuit indicator.

This technique estimates a single value of the resistance (R_s) (Figure 7), and thus it is not valid for asymmetric variations such as stator faults.

(b) shows inter-turn short-circuit indicator of R_s by classical technique (symmetric fault); (c) stator resistance estimation under inter-turn short-circuit fault (asymmetric fault); and (d) inter-turn short-circuit indicator of R_s by classical model reference adaptive system (MRAS) (asymmetric fault).

These results confirm the inability of the classical technique (classic MRAS) to provide information on the state of the machine.

8. The Proposed Estimation MRAS for the Per-phase Values Stator Resistance

Figure 8 shows the proposed technique based on a symmetrical PMSM in the (a, b, c) coordinate system; accordingly, the flux components generated by the permanent magnet are given as (Bouslimani et al. 2022, 2019, 2016) :

$$\begin{cases} \varphi_{ma} = \varphi_f \cos\theta \\ \varphi_{mb} = \varphi_f \cos\left(\theta + \dfrac{2\pi}{3}\right) \\ \varphi_{mc} = \varphi_f \cos\left(\theta + \dfrac{4\pi}{3}\right) \end{cases} \tag{48}$$

where φ_f is the flux linkage of the permanent magnet and θ is the electrical angular position.

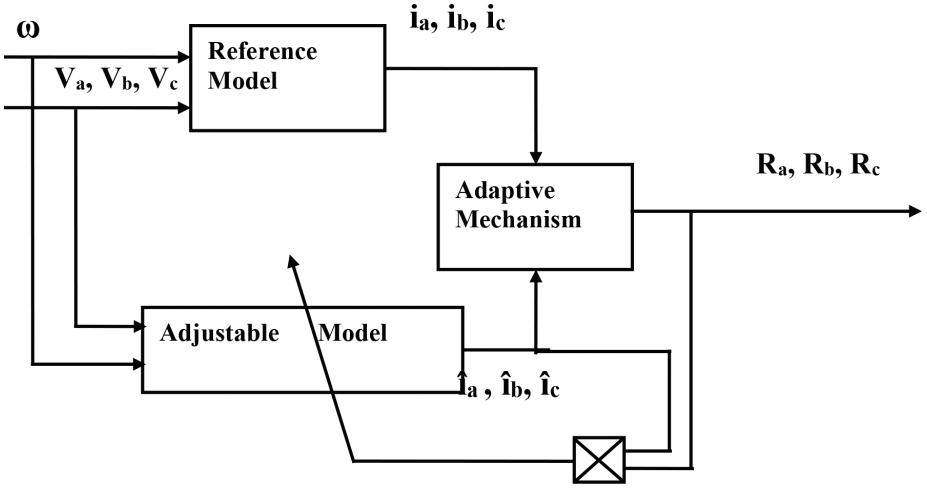

Fig. 8. MRAS stator resistances estimation.

The electrical motion equation of a PMSM, neglecting the reluctance effects, can be written as (Utkin et al., 2009):

$$\begin{cases} \dfrac{di_a}{dt} = -\dfrac{R_a}{L_a} i_a + \dfrac{1}{L_a} E_a - \dfrac{1}{L_a} u_a \\ \dfrac{di_b}{dt} = -\dfrac{R_b}{L_b} i_b + \dfrac{1}{L_b} E_b - \dfrac{1}{L_b} u_b \\ \dfrac{di_c}{dt} = -\dfrac{R_c}{L_c} i_c + \dfrac{1}{L_c} E_c - \dfrac{1}{L_c} u_c \end{cases} \tag{49}$$

where $R_{a,\,b,\,c}$ are the winding resistances, $L_{a,\,b,\,c}$ are the winding inductances, $i_{a,\,b,\,c}$ are the phases currents, and $u_{a,\,b,\,c}$ are the phase voltages.

Furthermore E_a, E_b, E_c are the induced electromotive force (EMF) components of the following form:

$$\begin{cases} E_a = -\varphi_f\ \omega \sin\theta \\ E_b = -\varphi_f\ \omega \sin\left(\theta + \dfrac{2\pi}{3}\right) \\ E_c = -\varphi_f\ \omega \sin\left(\theta + \dfrac{4\pi}{3}\right) \end{cases} \tag{50}$$

in which $\omega = \dfrac{d\theta}{dt}$ is the electrical angular speed.

Then, Eq. (2) can be expressed as:

$$\begin{cases} \dfrac{di_a}{dt} = -\dfrac{R_a}{L_a} i_a - \dfrac{1}{L_a} V_a \\ \dfrac{di_b}{dt} = -\dfrac{R_b}{L_b} i_b - \dfrac{1}{L_b} V_b \\ \dfrac{di_c}{dt} = -\dfrac{R_c}{L_c} i_c - \dfrac{1}{L_c} V_c \end{cases} \tag{51}$$

where,

$$\begin{aligned} V_a &= u_a - E_a \\ V_b &= u_b - E_b \\ V_c &= u_c - E_c \end{aligned}$$

$$\frac{d}{dt}\begin{bmatrix} i_a \\ i_b \\ i_c \end{bmatrix} = -\begin{bmatrix} \dfrac{R_a}{L} & 0 & 0 \\ 0 & \dfrac{R_b}{L} & 0 \\ 0 & 0 & \dfrac{R_c}{L} \end{bmatrix}\begin{bmatrix} i_a \\ i_b \\ i_c \end{bmatrix} - \begin{bmatrix} \dfrac{V_a}{L} \\ \dfrac{V_b}{L} \\ \dfrac{V_c}{L} \end{bmatrix} \tag{52}$$

An adjustable model can be obtained by substituting estimated value for real value in Eq. (5), and is given by:

$$\frac{d}{dt}\begin{bmatrix} \hat{i}_a \\ \hat{i}_b \\ \hat{i}_c \end{bmatrix} = -\begin{bmatrix} \dfrac{\hat{R}_a}{L} & 0 & 0 \\ 0 & \dfrac{\hat{R}_b}{L} & 0 \\ 0 & 0 & \dfrac{\hat{R}_c}{L} \end{bmatrix}\begin{bmatrix} \hat{i}_a \\ \hat{i}_b \\ \hat{i}_c \end{bmatrix} - \begin{bmatrix} \dfrac{V_a}{L} \\ \dfrac{V_b}{L} \\ \dfrac{V_c}{L} \end{bmatrix} \tag{53}$$

Subtracting Eq. (6) from Eq. (5), we obtain a form of Eq. (7), which is given by:

$$\begin{cases} \dot{e} = Ae + I.W \\ y = e \end{cases} \tag{54}$$

where

$$e=\begin{bmatrix} e_a & e_b & e_c \end{bmatrix}^T,\ e_a=(i_a-\hat{i}_a),\ e_b=(i_b-\hat{i}_b),\ e_c=(i_c-\hat{i}_c)$$

$$A=\begin{bmatrix} -\frac{R_a}{L} & 0 & 0 \\ 0 & -\frac{R_b}{L} & 0 \\ 0 & 0 & -\frac{R_c}{L} \end{bmatrix},\quad W=\begin{bmatrix} -\frac{\Delta R_a}{L} & 0 & 0 \\ 0 & -\frac{\Delta R_b}{L} & 0 \\ 0 & 0 & -\frac{\Delta R_c}{L} \end{bmatrix}\begin{bmatrix} \hat{i}_a \\ \hat{i}_b \\ \hat{i}_c \end{bmatrix}$$

We consider the following Lyapunov candidate function:

$$V=\frac{1}{2}e^Te+\frac{1}{2}\frac{(\Delta R_a)^2}{\lambda_a}+\frac{1}{2}\frac{(\Delta R_b)^2}{\lambda_b}+\frac{1}{2}\frac{(\Delta R_c)^2}{\lambda_c}>0$$

with:

$\lambda_a,\lambda_b,\lambda_c>0$ constants, which are involved in the Lyapunov function. Therefore, the derivative of the Lyapunov function is given as:

$$\dot{V}=e^T\dot{e}-\frac{\Delta R_a}{\lambda_a}\frac{d\hat{R}_a}{dt}-\frac{\Delta R_b}{\lambda_b}\frac{d\hat{R}_b}{dt}-\frac{\Delta R_c}{\lambda_c}\frac{d\hat{R}_c}{dt}$$

To ensure the negativity of the Lyapunov function, therefore ensuring convergence and stability of the process, we derive the following:

$$e^TW-\frac{\Delta R_a}{\lambda_a}\frac{d\hat{R}_a}{dt}-\frac{\Delta R_b}{\lambda_b}\frac{d\hat{R}_b}{dt}-\frac{\Delta R_c}{\lambda_c}\frac{d\hat{R}_c}{dt}=0$$

Finally, we have:

$$\begin{cases} \hat{R}_a=-\frac{\lambda_a}{L}\int e_a\,\hat{i}_a\,dt \\ \hat{R}_b=-\frac{\lambda_b}{L}\int e_b\,\hat{i}_b dt \\ \hat{R}_c=-\frac{\lambda_c}{L}\int e_c\,\hat{i}_c dt \end{cases}$$

$$\begin{cases} CC_a=\left(1-\frac{\hat{R}_a}{R_s}\right)100 \\ CC_b=\left(1-\frac{\hat{R}_b}{R_s}\right)100 \\ CC_c=\left(1-\frac{\hat{R}_c}{R_s}\right)100 \end{cases}$$

9. Simulation Results

In order to verify the proposed fault diagnosis technique, simulations were performed for variable speed. The Figures 9 (a) and (b) show the simulation results of the proposed MRAS technique with inter turn short circuits.

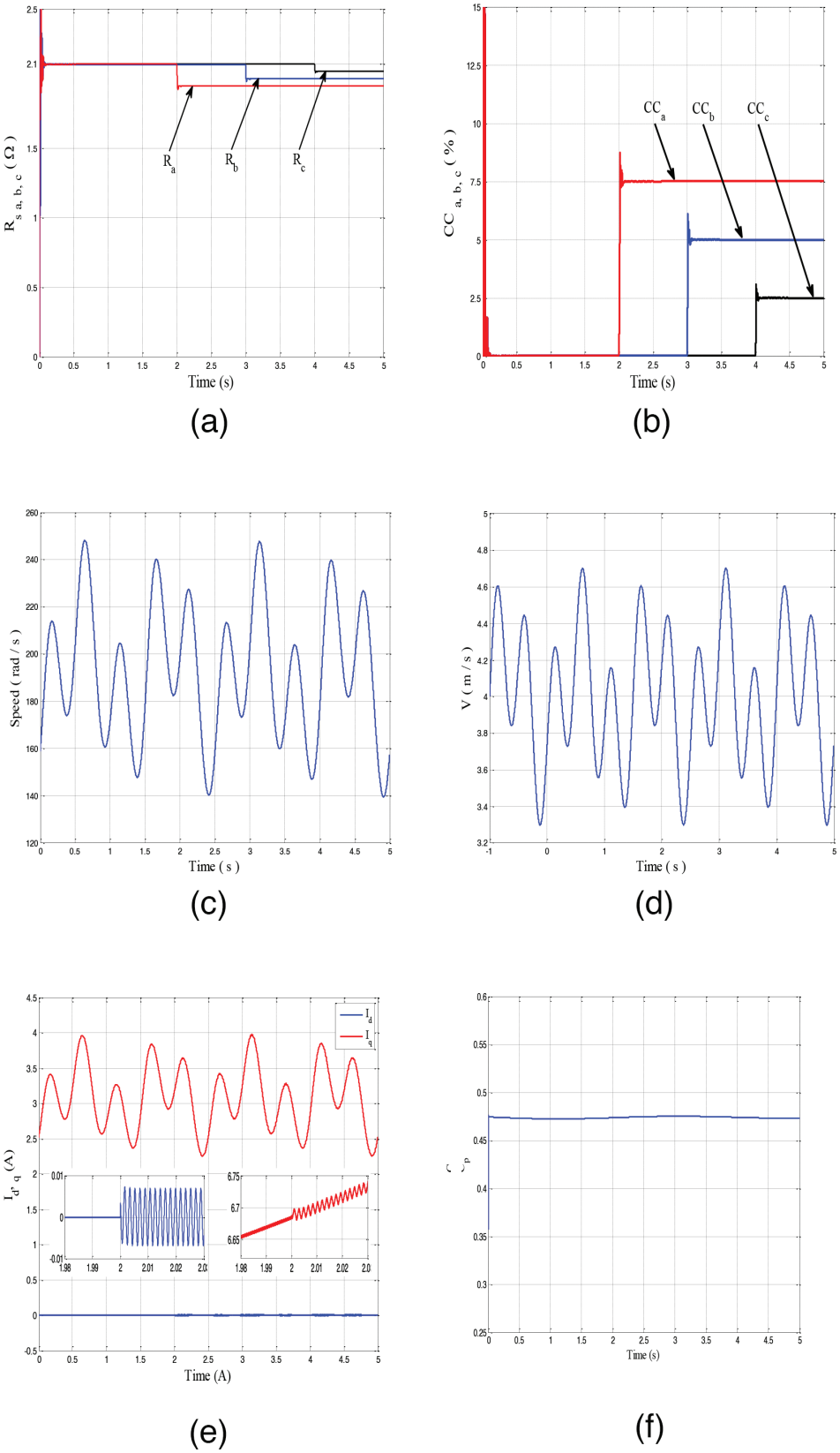

Fig. 9. (a) Estimated stator resistances under inter-turn short-circuit fault, (b) inter turn short circuit indicator, (c) mechanical speed, (d) wind speed profile, (e) direct and quadrature currents, and (f) power coefficient.

Figure 9 (c) shows the performance of MRAS rotor speed estimator with taking consideration of stator inter-turn short-circuits. Figure 9 (d) shows the evolution of the main characteristics namely: direct and quadrature currents with taking consideration of stator inter-turn short-circuits.

10. Conclusion

In this paper, principally with the objective of estimating the resistance value of each phase of PMSG in WECS, we propose a fast and robust fault diagnosis strategy in closed-loop using the direct Lyapunov control in conjunction with the MRAS technique. The proposed scheme has been achieved by using the variation of the stator resistances, which are estimated in real time to detect the faulty phase with fastest time and can easily be embedded. The robustness and stability are guaranteed theoretically and illustrated. The feasibility of the proposed fault diagnosis scheme has been verified using simulation results under various fault conditions. However, there are several areas of future research that can be explored to further enhance the efficiency and robustness of the strategy.

1. Investigation of fault scenarios: The fault diagnosis strategy should be able to detect different types of faults that may occur in the WECS, including rotor faults, stator faults, and power electronic faults.
2. Improved MRAS technique: The effectiveness of the MRAS technique in estimating the resistance value of each phase of PMSG is crucial for the accuracy of the fault diagnosis strategy. Therefore, future research can focus on developing improved MRAS techniques that can provide more accurate estimation of the resistance value under different operating conditions.
3. Robustness analysis: The robustness of the fault diagnosis strategy in the presence of measurement noise, parameter uncertainties, and modelling errors is an important consideration.
4. Validation using experimental data: This methodology involves developing experimental setups that can accurately represent the dynamics of a WECS and conducting experiments to validate the proposed strategy.
5. Integration with other control strategies: The fault diagnosis strategy can be integrated with other control strategies, such as fault-tolerant control and reconfiguration control, to enhance the overall performance of the WECS.

References

Ackermann, J. (1980). Parameter Space Design of Robust Control Systems. *IEEE Transactions on Automatic Control*, AC-25(6), pp. 1058–1072.

Ackermann, J. (1985). *Sampled-Data Control Systems: Analysis and Synthesis, Robust System Design*. Berlin: Springer Eds.

Ameur, A., Mokhtari, B., Essounbouli, N. and Mokrani, L. (2012). Speed Sensorless Direct Torque Control of a PMSM Drive using Space Vector Modulation Based MRAS and Stator Resistance Estimator. *World Academy of Science, Engineering and Technology*, Vol:6, No:6, 2012

Amirat, Y., Benbouzid, M. E. H., Al-Ahmar, E., Bensaker, B. and Turri, S. (2009). A Brief Status on Condition Monitoring and Fault Diagnosis in Wind Energy Conversion Systems. *Renewable and Sustainable Energy Reviews*, 13(9) : 2629-2636

Barut, M., Hinkkanen, M. and Orłowska-Kowalska, T. (2018). Introduction to the Special Section on State and Parameter Estimation Methods for Sensorless Drives. *Power Electronics and Drives*, 3(38), pp. 111–113. doi: 10.2478/pead-2018-0018.

Beltran, B., Benbouzid, M. E. H. and Ahmed-Ali, T. (2009). High-order sliding mode control of a DFIG-based wind turbine for power maximization and grid fault tolerance. In: *IEEE International Electric Machines and Drives Conference (IEMDC)*, Miami, FL, USA.

Bonnett, H. A. (1978). Analysis of Winding Failures in Three-Phase Squirrel Cage Induction Motors. *IEEE Transactions on Industry Applications*, 14(3), pp. 223–226.

Bouslimani, S., Chrifi-Alaoui, L., Merad, S., Delahoche, L., Bussy, P. and Drid, S. (2022). Stator fault detection of the PMSG under the sliding mode control in wind energy conversion system. In: *Conference: 2022 IEEE 21st International Conference on Sciences and Techniques of Automatic Control and Computer Engineering (STA)*. Sousse, Tunisia, doi: 10.1109/STA56120.2022.10019025.

Bouslimani, S., Drid, S. and Chrifi-Alaoui, L. (2019). Sensorless Control and Diagnosis of Synchronous-Generator used in Wind Energy Conversion System Under Inter Turn Short-Circuit

Fault. *International Journal of Power and Energy Conversion (IJPEC)*, 10(4), p. 480. doi: 10.1504/IJPEC.2019.10012581.

Bouslimani, S., Drid, S., Chrifi-Alaoui, L., Bussy, P. and Hamzaoui, M. (2016). Inter-turn faults detection using park vector strategy. In: *The 17th International Conference on Sciences and Techniques of Automatic Control & Computer Engineering (STA)*, Sousse, Tunisia, 18–21 December 2016. doi: 10.1109/STA.2016.7952082.

Brandao, R. M., Carvalho, J. B. and Barbosa, F. M. (2008). Fault detection on wind generators. In: *43rd International Universities Power Engineering Conference (UPEC)*. Padua, Italy.

Costa, M. A. A., Braga-Filho, E. R. and Lima, A. M. N. (2013). Designing a low cost high performance permanent magnet motor drive system. In: *IECON 2013 – 39th Annual Conference of the IEEE Industrial Electronics Society*, Vienna, Austria, 10–13 November 2013, pp. 2738–2743. doi: 10.1109/IECON.2013.6699564.

Ekanayake, J. B., Holdsworth, L., Wu, X. G. and Jenkins, N. (2003). Dynamic Modeling of Doubly Fed Induction Generator Wind Turbines. *IEEE Transaction on Power System*, 18(2), pp. 803–809.

Fetene, Y. and Shibeshi, D. (2020). Fractional Order Sliding Mode Speed Control of Feedback Linearized Induction Motor. *Power Electronics and Drives*, 5(40), pp. 109–122. doi: 10.2478/pead-2020-0010.

Ghosh, B. K. (1986). Simultaneous Partial Pole Placement: New Approach to Multimode System Design. *IEEE Transactions on Automatic Control*, AC-31, pp. 440–443.

Hajji, S., Chehida, R. B., Zayani, H., Bouaziz, N. and Agrebi Zorgani, Y. (2020). Sensorless Induction Motor Drive Based on Model Reference Adaptive System Scheme Utilising a Fictitious Resistance. *Power Electronics and Drives*, 5(40), pp. 199–213. doi: 10.2478/pead-2020-0015.

Kallesoe, C. S., Vadstrup, P., Rasmussen, H. and Izadi-Zamanabadi, R. (2004). Estimation of Stator Winding Faults in Induction Motors using an Adaptive Observer Scheme. *IEEE Industry Applications Conference*, 2, pp. 1225–1232. doi: 10.1109/IAS.2004.1348569.

Meradi, S., Benmansour, K., Herizi, K., Tadjine, M. and Boucherit, M. S. (2013). Sliding Mode and Fault Tolerant Control For Multicell Converter Four Quadrants. *Electric Power Systems Research*, 95, 128–139. doi: 10.1016/j.epsr.2012.08.014.

Meradi, S., Benmansour, K., Tadjine, M. M. S. and Boucherit, Z. (2022). Observability Concept Analysis for Power Flying Capacitors of Multicells Converters. *Electric Power Components and Systems*, 49(11-12), pp. 1021–1033. doi: 10.1080/15325008.2021.2013994.

Nguyen, H. M. and Naidu, D. S. (2011) Advanced control strategies for wind energy systems. In: *IEEE PES Power Systems Conference & Exposition (PSCE)*, Phoenix, 20–23 March 2011, pp. 1–8. doi: 10.1109/PSCE.2011.5772514.

Robyns, B. (1992). Commande numerique desmoteurs asynchrone et asynchrone', Seminaire sur les entrainements à vitesse variable', Rabat, Maroc.

Utkin, V., Guldner, J. and Shi, J. (2009). *Sliding Mode Control in Electro-Mechanical Systems*. CRC Press, Boca Raton, Taylor and Francis Group.

Wang, Y. and Deng, Z. (2012). Hybrid Excitation Topologies and Control Strategies of Stator Permanent Magnet Machines for DC Power System. *IEEE Transactions on Industrial Electronics*, 59(12), pp. 4601–4616. doi: 10.1109/TIE.2012.2183842.

Weeber, K. R., Shah, M. R., Sivasubramaniam, K., El-Refaie, A., Qu, R., Stephens, C. and Galioto, S. (2010). Advanced permanent magnet machines for a wide range of industrial applications. In: *Proceedings of IEEE PES General Meeting*, pp. 1–6, Minneapolis, MN, USA, July 2010.

Yin, M., Li, G., Zhou, M. and Zhao, C. (2007). Modeling of the wind turbine with a permanent magnet synchronous generator for integration. In: *IEEE Power Engineering Society General Meeting*, Tampa, 24–28 June 2007, pp. 1–6. doi: 10.1109/PES.2007.385982.